

The obstacle problem in watertable–ground interaction¹

HÉLOISE BEAUGENDRE² and ALEXANDRE ERN

Cermics, Ecole nationale des ponts et chaussées
6 et 8 avenue Blaise Pascal, 77455 Marne-la-Vallée, France
ern@cermics.enpc.fr

1 Introduction

The prediction of overland flow routing in hillslopes is of paramount importance during flood episodes. Owing to the complexity of the problem, in situ experiments are often difficult to perform and general conclusions are difficult to draw. This has prompted the development of numerical tools with the capability to analyze water transfer in virtual hillslopes subjected to various operating conditions. This approach has experienced a vigorous development over the past decades. Many advances have been reported in the specialized literature, concerning both the development of models describing the hydrological behavior of hillslopes through partial differential equations (PDEs) and appropriate boundary conditions (BCs) and the design of suitable numerical methods able to tackle such PDEs and BCs. Recent work in this direction includes, among others, Ogden & Watts [1], Cloke *et al.* [2], and Weiler & McDonnell [3].

An important aspect of hillslope hydrology during heavy rainfall episodes is the fact that subsurface flows can saturate the soil in various regions near the surface and, therefore, contribute to the production of overland flow. There is therefore a strong motivation to improve our understanding of subsurface flow dynamics in variably saturated porous media and, in particular, of the role played by the hydraulic state of the soil in storm hydrographs. As part of an ongoing research effort in that direction, this paper discusses numerical tools, essentially based on finite element techniques, to discretize various PDEs relevant to hillslope hydrology models, and presents some selected results illustrating the interaction of subsurface flow dynamics with the ground surface.

Section 2 presents a model often considered to describe unsteady flows in variably saturated porous media, namely Richards' equation. Richards' equation requires two algebraic relations to model the hydrodynamic behavior of the soil. These relations relate the unsaturated hydraulic conductivity, the volumetric water content, and the hydraulic head. Section 2 also addresses in some detail the case where the water-table (i.e., that part of the soil where saturation takes place) reaches the top boundary of the hillslope, i.e., the ground surface. Since the water-table position is an unknown of the problem, its intersection with the ground surface is a priori unknown. This leads to an unsteady obstacle-type problem.

Section 3 discusses the modeling of overland flow on the ground surface. Two simplified forms of the Saint-Venant equations are considered, namely the diffusive wave approximation and the kinematic wave approximation. Numerical algorithms coupling the overland flow with subsurface flows governed by Richards' equation are also presented.

Finally, Section 4 presents some selected results on hillslope behavior during heavy rainfall episodes. It discusses the impact of phenomenological parameters on model predictions and

¹Part of this work has been carried in collaboration with the research units Hban/Cemagref, Cereve/Enpc, and Estime/Inria in the framework of the Cooperative Research Action DYNAS sponsored by INRIA; see <http://www-rocq.inria.fr/estime/DYNAS>

²Current address: MAB, Université Bordeaux I, 351, cours de la Libération, 33405 Talence, France

compares two approaches to simulate the subsurface flow, one neglecting the height of the overland flow in the specification of BCs for Richards' equation and the other taking it into account.

2 Finite elements for variably saturated flows

This section focuses on Richards' equation to model variably saturated flows. Some emphasis is set on the finite element formulation in the case where the water-table reaches the ground surface, thus leading to an obstacle-type problem for the hydraulic head.

2.1 Richards' equation

In an unsaturated porous medium, the fluid phase contains water and air. The most general approach to model flows through such media is to address the two-phase problem by considering mass and momentum balance for each of the two phases; see, e.g., [9]. However, a simpler approach is feasible if the gas-phase always remains connected so that a single air pressure can be considered. This is the first important assumption underlying Richards' equation. Hence, entrapped air pockets are excluded from the present configuration.

Let θ be the volumetric water content and let φ be the (total) hydraulic head. Set

$$\varphi = \psi + z, \quad (1)$$

where z is the vertical coordinate (oriented upwards) and ψ is the so-called matrix potential. This quantity is related to the difference between air pressure and water pressure in such a way that $\psi < 0$ in unsaturated regions and $\psi > 0$ in saturated regions. The water-table position is located at the isoline $\{\psi = 0\}$.

The second assumption underlying Richards' equation is that a generalized Darcy's law relates the water flow velocity to the hydraulic head gradient through the concept of relative hydraulic conductivity. In other words, it is assumed that

$$u = -k_s k_r(\theta) \nabla \varphi, \quad (2)$$

where k_s is the hydraulic conductivity at saturation (i.e., the hydraulic conductivity pertinent for Darcy's equation) and $k_r(\theta)$ is the so-called relative hydraulic conductivity that depends on the volumetric water content θ . For the sake of simplicity, the medium is assumed to be isotropic so that a single scalar hydraulic conductivity can be considered instead of a full tensor. As a result, the water conservation equation $\partial_t \theta + \nabla \cdot u = f$ takes the form

$$\partial_t \theta - \nabla \cdot (k_s k_r(\theta) (\nabla \psi + e_z)) = f, \quad (3)$$

where e_z is the unit vector oriented upwards and where f represents the volumetric water sources or sinks in Ω .

To close the problem, it is necessary to assume that an algebraic relation links the volumetric water content θ to the matrix potential ψ , say $\psi \mapsto \theta(\psi)$. The graph of the function $\psi \mapsto \theta(\psi)$ is often called the soil water retention curve. Equation (3) then yields a PDE where the sole dependent variable is the matrix potential ψ , namely,

$$\partial_t \theta(\psi) - \nabla \cdot (k_s k_r(\theta(\psi)) (\nabla \psi + e_z)) = f. \quad (4)$$

This PDE can be written in mixed form by introducing the generalized Darcy velocity $u(\psi)$,

$$\begin{cases} \partial_t \theta(\psi) + \nabla \cdot u(\psi) = f, \\ u(\psi) + k_s k_r(\theta(\psi)) (\nabla \psi + e_z) = 0. \end{cases} \quad (5)$$

To enforce boundary conditions for (4) or (5), assume that the boundary $\partial\Omega$ can be partitioned into $\partial\Omega_1 \cup \partial\Omega_2$ in such a way that the hydraulic head is imposed on $\partial\Omega_1$ and that a

normal velocity is prescribed on $\partial\Omega_2$. This yields

$$\psi = g_1 - z \quad \text{on } \partial\Omega_1, \quad (6)$$

$$-k_s k_r(\theta(\psi))(\nabla\psi + e_z) \cdot n = g_2 \quad \text{on } \partial\Omega_2, \quad (7)$$

where n is the outward normal to Ω . In other words, Dirichlet and (nonlinear) Neumann conditions are imposed on ψ . A more complex situation where the partition $\partial\Omega_1 \cup \partial\Omega_2$ is not known a priori is discussed in Section 2.4.

Finally, (4) or (5) is supplied with an initial condition specifying the initial value of the matrix potential, namely

$$\psi = \psi_0 \quad \text{at } t = 0 \text{ and in } \Omega. \quad (8)$$

2.2 Soil hydrodynamic functions

In soils, the volumetric water content does not vary between 0 and 1, but between a minimum value θ_r called the residual volumetric water content and a maximum value θ_s called the saturated volumetric water content. Define the reduced volumetric water content

$$\tilde{\theta} = \frac{\theta - \theta_r}{\theta_s - \theta_r}, \quad (9)$$

which, by definition, varies between 0 and 1.

A model often considered in the engineering literature to specify the soil water retention curve is that derived by van Genuchten in 1980 [10]

$$\tilde{\theta}(\psi) = \begin{cases} (1 + (-\alpha\psi)^n)^{-m}, & \psi < 0, \\ 1, & \psi \geq 0, \end{cases} \quad (10)$$

with $m = 1 - \frac{1}{n}$. Equation (10) involves two parameters, α and n . It should be noted that if the exponent n is less than 2, the function $\psi \mapsto \tilde{\theta}(\psi)$ is only of class C^1 at $\psi = 0$ and its second-derivative explodes as $\psi \rightarrow 0^-$, whereas for $n \geq 2$, the function $\psi \mapsto \tilde{\theta}(\psi)$ is of class C^2 at $\psi = 0$. This fact can be important in numerical approaches where the volumetric water content is chosen as the main dependent variable for (4).

A model to express the relative hydraulic conductivity has been proposed by Mualem in 1976 [11],

$$k_r(\tilde{\theta}) = \tilde{\theta}^l \left(\frac{\int_0^{\tilde{\theta}} \psi(\tau)^{-1} d\tau}{\int_0^1 \psi(\tau)^{-1} d\tau} \right)^2, \quad (11)$$

where l is the pore connectivity parameter (generally set to $l = \frac{1}{2}$) and $\tau \mapsto \psi(\tau)$ denotes the reciprocal function of $\psi \mapsto \tilde{\theta}(\psi)$. Combined with (10), the Mualem relation yields

$$k_r(\tilde{\theta}) = \tilde{\theta}^{\frac{1}{2}} \left(1 - (1 - \tilde{\theta}^{\frac{1}{m}})^m \right)^2. \quad (12)$$

Equations (10) and (12) are referred to as the Van Genuchten–Mualem (VGM) model. In the framework of the VGM model, a soil is described by five parameters: k_s , α , n , θ_s , and θ_r .

Recently, it was observed that relatively small changes in the shape of the soil water retention curve near saturation could significantly affect the numerical performance of variably saturated flow simulations [12]. As a result, a modified form of the VGM model was proposed to account for a very small, but non-zero, minimum capillary height, $\psi_s < 0$, in the soil water retention curve. This modification leads to less non-linearity in the hydraulic conductivity function near saturation and, hence, to more stable numerical solutions. The modified VGM model takes the following form:

$$\tilde{\theta}(\psi) = \begin{cases} \beta (1 + (-\alpha\psi)^n)^{-m}, & \psi < \psi_s, \\ 1, & \psi \geq \psi_s, \end{cases} \quad (13)$$

where the parameter β is defined as $\beta = (1 + (-\alpha\psi_s)^n)^{-m}$ in such a way that $\tilde{\theta}(\psi_s) = 1$. Furthermore, the relative hydraulic conductivity dependency on $\tilde{\theta}$ is modified so that its dependency on ψ is unchanged if (13) replaces (10). This leads to

$$k_r(\tilde{\theta}) = \tilde{\theta}^{\frac{1}{2}} \left[1 - \left(1 - (\beta^{-1}\tilde{\theta})^{\frac{1}{m}} \right)^m \right]^2 \left[1 - \left(1 - \beta^{-\frac{1}{m}} \right)^m \right]^{-2}. \quad (14)$$

Equations (13) and (14) reduce to the original VGM model when $\psi_s = 0$ (and, hence, $\beta = 1$). Equation (14) bears some similarity with the well-known Brooks–Corey model [13] relating the relative hydraulic conductivity to the matrix potential in the form

$$k_r(\psi) = \left(\frac{\psi}{\psi_s} \right)^{-\varrho}, \quad \psi \leq \psi_s < 0, \quad (15)$$

where ψ_s is the minimum capillary height and ϱ is a suitable parameter.

Although the approach leading to Richards’ equation is attractive since it reduces the variably saturated flow problem to a single PDE, it requires two algebraic relations for its closure, and this presents two drawbacks. Firstly, phenomenological parameters must be supplied to specify the soil hydrodynamic functions. For instance, five parameters are required in the VGM model and six in the modified VGM model. These parameters are often difficult to determine experimentally, but can have a significant impact on model predictions. This issue will be further discussed in Section 4. The second drawback is that field experiments indicate that the functions $\psi \mapsto \theta(\psi)$, $\psi \mapsto k_r(\psi)$, and $\theta \mapsto k_r(\theta)$ are not single-valued. Instead, an hysteresis behavior is often observed depending on whether the water content in the soil is decreased or increased. Hence, the use of the above models implicitly assumes that the volumetric water content is monotone during the simulation.

2.3 Space and time discretization

Many strategies to approximate Richards’ equation are feasible depending on the choice for the primal unknown, of the non-linear iterative solver, and of the space and time discretization scheme; see, e.g., Celia *et al.* [14].

In the present work, we focus on some specific choices. Firstly, the matrix potential ψ is retained as the primal unknown. Secondly, the so-called *method of lines* is employed for the time-space discretization: the problem is first approximated in space using (for instance) finite element methods, thereby yielding a system of coupled ordinary differential equations (ODEs) where the time is the only independent variable. Then, a time approximation is constructed by using the vast theory of solution techniques for ODEs; see, e.g. [15] for a thorough review. Finally, Newton’s method is used as the iterative solver to obtain an approximate solution to the non-linear discrete equations.

We briefly describe a standard finite element approximation to Richards’ equation. Consider the primal form (4) of Richards’ equation. Up to an appropriate lifting of the boundary data g_1 and a modification of the right-hand side f , we can assume that a homogeneous Dirichlet boundary condition is prescribed on $\partial\Omega_1$. Set

$$V_{\partial\Omega_1} = \{ \phi \in H^1(\Omega); \phi = 0 \text{ on } \partial\Omega_1 \}, \quad (16)$$

and let a_R be the form (non-linear in ψ , linear in ϕ):

$$a_R(\psi, \phi) = \int_{\Omega} \partial_t \theta(\psi) \phi + \int_{\Omega} k_s k_r(\theta(\psi)) (\nabla \psi + e_z) \cdot \nabla \phi. \quad (17)$$

Then, a possible weak formulation of (4) is the following:

$$\begin{cases} \text{Seek } \psi \in C^1([0, T]; V_{\partial\Omega_1}) \text{ such that, for all } t \geq 0, \\ a_R(\psi, \phi) = \int_{\Omega} f \phi - \int_{\partial\Omega_2} g_2 \phi, \quad \forall \phi \in V_{\partial\Omega_1}, \end{cases} \quad (18)$$

where $C^1([0, T]; V_{\partial\Omega_1})$ is the space of functions in time with values in $V_{\partial\Omega_1}$ that are of class C^1 in time, and T is a fixed simulation time.

To approximate (18), consider conforming, piecewise linear finite elements. Assume that the mesh \mathcal{T}_h is compatible with the partition $\partial\Omega_1 \cup \partial\Omega_2$, i.e., that $\partial\Omega_1 \cap \partial\Omega_2$ consists of mesh vertices (and edges in three dimensions). Introduce the finite element space

$$P_{c, \partial\Omega_1}^1 = \{ \phi_h \in C^0(\bar{\Omega}); \forall K \in \mathcal{T}_h, \phi_h|_K \in \mathbb{P}_1; \phi_h = 0 \text{ on } \partial\Omega_1 \}. \quad (19)$$

The conforming approximation of Richards' equation in primal form is the following:

$$\begin{cases} \text{Seek } \psi_h \in C^1([0, T]; P_{c, \partial\Omega_1}^1) \text{ such that, for all } t \geq 0, \\ a_R(\psi_h, \phi_h) = \int_{\Omega} f \phi_h - \int_{\partial\Omega_2} g_2 \phi_h, \quad \forall \phi_h \in P_{c, \partial\Omega_1}^1. \end{cases} \quad (20)$$

To approximate (20) in time, we restrict the discussion to the implicit Euler scheme. Let δt be the time step and define

$$a_{R, \delta t}(\psi, \phi) = \int_{\Omega} \theta(\psi) \phi + \delta t \int_{\Omega} k_s k_r(\theta(\psi)) (\nabla \psi + e_z) \cdot \nabla \phi. \quad (21)$$

Let $\psi_h^0 \in P_{c, \partial\Omega_1}^1$ be a suitable approximation to the initial value ψ_0 , e.g., the L^2 -orthogonal projection of ψ_0 onto $P_{c, \partial\Omega_1}^1$ or its Lagrange interpolant. Then, the time-marching scheme consists of generating the sequence of approximations $\psi_h^n \in P_{c, \partial\Omega_1}^1$, $n \geq 1$, where ψ_h^n is an approximation of ψ at time $t^n = n\delta t$, by solving sequentially in time the following problems: For $n \geq 1$,

$$\begin{cases} \text{Seek } \psi_h^n \in P_{c, \partial\Omega_1}^1 \text{ such that} \\ a_{R, \delta t}(\psi_h^n, \phi_h) = \delta t \int_{\Omega} f \phi_h - \delta t \int_{\partial\Omega_2} g_2 \phi_h + \int_{\Omega} \theta(\psi_h^{n-1}) \phi_h, \quad \forall \phi_h \in P_{c, \partial\Omega_1}^1. \end{cases} \quad (22)$$

2.4 Water-table-ground interaction and the obstacle problem

To investigate water-table-ground interaction, we consider a simplified problem: the domain Ω is a quadrangle, no-flux conditions are imposed on the left, bottom, and right boundaries, and the top boundary, $\partial\Omega_g$, is exposed to a constant rainfall with velocity $v_r = -ie_z$ where $i > 0$ is the rainfall intensity; see Figure 1. In this setting, $\partial\Omega_g$ coincides with the ground surface. Henceforth, it is assumed that $i \leq k_s$, i.e., that the rainfall intensity never exceeds the infiltration capacity of the soil.

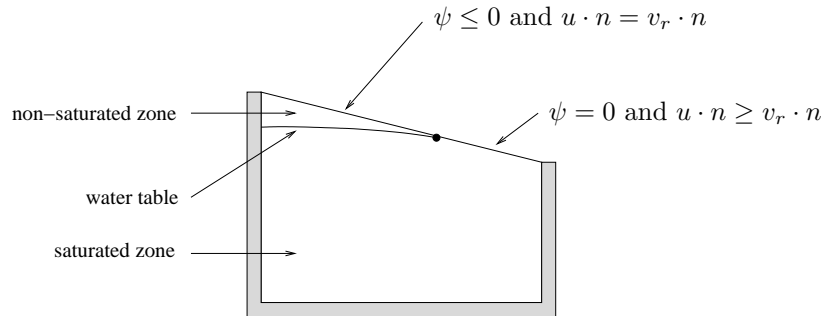


Figure 1: Setting for water-table-ground interaction.

Assume that initially the water-table does not intersect the ground surface. Then, the boundary condition is $u \cdot n = v_r \cdot n$ throughout $\partial\Omega_g$, i.e., a non-homogeneous Neumann boundary condition expressing the fact that the rainfall infiltrates inside the soil. As a result, the

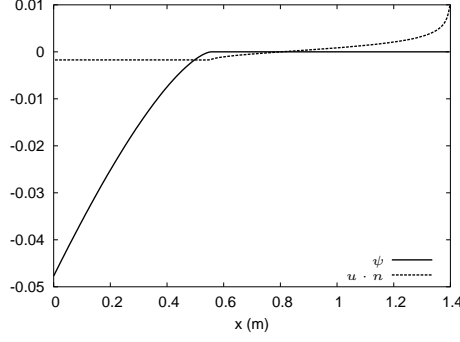


Figure 2: Matrix potential (solid) and normal flow velocity (dash) along the ground surface.

volumetric water content in the soil increases, and the water-table moves upwards until it reaches the ground surface. Once the water-table intersects the ground surface, the following holds on $\partial\Omega_g$:

$$\psi \leq 0, \quad u \cdot n \geq v_r \cdot n, \quad \psi(u \cdot n - v_r \cdot n) = 0, \quad (23)$$

so that the ground surface can be divided into two regions

- $\partial\Omega_g^-$ corresponds to the non-saturated part of $\partial\Omega_g$: $\psi < 0$ and $u \cdot n = v_r \cdot n$;
- $\partial\Omega_g^+$ corresponds to the saturated part of $\partial\Omega_g$: $\psi = 0$ and $u \cdot n > v_r \cdot n$.

An important assumption in this model is that the height of the overland flow above the ground surface is neglected so that the boundary condition in $\partial\Omega_g^+$ is indeed $\psi = 0$. A model accounting for the coupling between the water-table dynamics and the overland flow will be discussed in Section 3.

Figure 2 presents an example of profiles for the matrix potential and the normal flow velocity along the ground surface. The point where the water-table intersects the ground surface is clearly visible and corresponds to a longitudinal abscissa of approximately 0.55 m. It is also observed that the saturated part $\partial\Omega_g^+$ can be further divided into two subregions,

- one part still allows for some infiltration: $\psi = 0$ and $v_r \cdot n < u \cdot n < 0$;
- the other part corresponds to the exfiltration region: $\psi = 0$ and $u \cdot n > 0$.

To investigate the formulation of Richards' equation (4) together with the obstacle boundary condition (23), we consider first a steady setting and then an unsteady setting.

2.4.1 Steady obstacle problem

Given $\partial\Omega_g^+ \subset \partial\Omega_g$, let $P_{c,\partial\Omega_g^+}^1$ be defined as in (19) and let

$$a_{\partial\Omega_g^+}(\psi, \phi) = \int_{\Omega} k_s k_r(\theta(\psi)) (\nabla\psi + e_z) \cdot \nabla\phi + \int_{\partial\Omega_g^-} (v_r \cdot n) \phi. \quad (24)$$

Note that working with the space $V_{\partial\Omega_g^+}$ implies $\psi = 0$ on the saturated part $\partial\Omega_g^+$.

The discrete steady obstacle problem consists of seeking a pair $\{\partial\Omega_g^+, \psi_h\}$ such that

$$\partial\Omega_g^+ \subset \partial\Omega_g, \quad (25)$$

$$\psi_h \in P_{c,\partial\Omega_g^+}^1, \quad (26)$$

$$a_{\partial\Omega_g^+}(\psi_h, \phi_h) = 0 \quad \forall \phi_h \in P_{c,\partial\Omega_g^+}^1, \quad (27)$$

$$\psi_h \leq 0 \quad \text{on } \partial\Omega_g^-, \quad (28)$$

$$u(\psi_h) \cdot n \geq v_r \cdot n \quad \text{on } \partial\Omega_g^+. \quad (29)$$

The well-posedness of (27) requires that $\partial\Omega_g^+ \neq \emptyset$, i.e., that the water-table has reached the ground surface.

An approximate solution $\{\partial\Omega_g^+, \psi_h\}$ of (25)–(29) is sought using Newton’s method embedded into a fixed-point iteration to determine the intersection of the water-table with the ground surface. The following iterative algorithm is proposed to solve the problem:

1. choose an initial $\partial\Omega_g^+$;
2. solve problem (27);
3. check whether (28) and (29) are satisfied;
4. if (28) is satisfied and (29) is not, decrease $\partial\Omega_g^+$ by one or more mesh cells; go to step 2;
5. if (29) is satisfied and (28) is not, increase $\partial\Omega_g^+$ by one or more mesh cells; go to step 2;
6. if both (28) and (29) are satisfied, then the current pair $\{\partial\Omega_g^+, \psi_h\}$ is the desired solution; one can refine the mesh and go back to step 2.

Owing to the maximum principle, both (28) and (29) can not be violated simultaneously. However, in numerical approximations, this can happen. In this case, we still consider that the water-table has been correctly positioned. With this “loosened” convergence criterion, the final position of the water-table depends from whether the converged $\partial\Omega_g^+$ has been approached from below or above. The two resulting values give lower and upper bounds for the water-table position (typically differing from one or two mesh cells at the most).

2.4.2 Unsteady obstacle problem

The unsteady version of the above obstacle problem can be implemented using an implicit Euler scheme. For $n \geq 1$, given $(\partial\Omega_g^+)^{n-1}$ and ψ_h^{n-1} , seek $\{(\partial\Omega_g^+)^n, \psi_h^n\}$ such that

$$(\partial\Omega_g^+)^n \subset \partial\Omega_g, \quad (30)$$

$$\psi_h^n \in P_{c,(\partial\Omega_g^+)^n}^1, \quad (31)$$

$$\frac{1}{\delta t} \int_{\Omega} (\theta(\psi_h^n) - \theta(\psi_h^{n-1})) \phi_h + a_{(\partial\Omega_g^+)^n}(\psi_h^n, \phi_h) = 0 \quad \forall \phi_h \in P_{c,(\partial\Omega_g^+)^n}^1, \quad (32)$$

$$\psi_h^n \leq 0 \quad \text{on } (\partial\Omega_g^-)^n, \quad (33)$$

$$u(\psi_h^n) \cdot n \geq v_r \cdot n \quad \text{on } (\partial\Omega_g^+)^n. \quad (34)$$

This problem can be solved using the same iterative algorithm as for the steady obstacle problem. In step 1, the initial choice is $(\partial\Omega_g^+)^n = (\partial\Omega_g^+)^{n-1}$. Note that in the unsteady case, problem (32) is well-posed even if the water table has not reached the top boundary yet.

3 Overland flow

This section briefly presents some models that can be used to describe overland flow over hillslopes. The coupling with Richards’ equation is also discussed.

3.1 Model formulation

Transient flow of shallow water can be modelled by the Saint-Venant equations. To simplify, we consider a two-dimensional hillslope model; the overland flow then reduces to a one-dimensional problem governed by the following equations:

$$\partial_t y + \partial_x(yV) = w, \quad (35)$$

$$\partial_t V + V\partial_x V + g\partial_x y + g(S_f - S) = 0, \quad (36)$$

were y is the water depth, V the flow velocity, w the source term, g the gravity, S the river bed slope, and S_f the energy line slope.

We assume that in the momentum equation (36), the first two terms, i.e., the inertia terms, can be neglected in comparison with the last two terms. This yields the so-called *diffusive wave approximation*

$$\partial_t y + \partial_x(yV) = w, \quad (37)$$

$$\partial_x y + S_f - S = 0. \quad (38)$$

This model is widely used to describe flood routing; see, e.g., [16].

The Manning–Strickler uniform flow formula is usually chosen to evaluate the energy line slope S_f [17, 18], namely

$$V = K_S R^{\frac{2}{3}} \operatorname{sgn}(S_f) |S_f|^{\frac{1}{2}}, \quad (39)$$

where K_S is the Strickler coefficient of roughness and R is the hydraulic radius defined as the ratio between the cross-sectional flow area, A , and the wet perimeter, χ . Assuming that the overland flow occurs as a thin layer with a wide rectangular section of width B yields the relation $y \ll B$. Hence, $A = By$, $\chi = B + 2y$, and

$$R = \frac{By}{B + 2y} \approx y. \quad (40)$$

Let $q(y) = yV$. Using equations (38) and (40) in (39) yields

$$q(y) = K_S y^{\frac{5}{3}} \operatorname{sgn}(S_f) |S - \partial_x y|^{\frac{1}{2}}. \quad (41)$$

The continuity equation then becomes the so-called *diffusive wave equation*

$$\partial_t y + \partial_x \left(K_S y^{\frac{5}{3}} \frac{S - \partial_x y}{|S - \partial_x y|^{\frac{1}{2}}} \right) = w. \quad (42)$$

One advantage of the diffusive wave approximation is to reduce the Saint-Venant equations to a single PDE. However, by doing so, the differential order of the PDE is increased, and it is necessary to supply two boundary conditions to close (42).

A further simplification with respect to the diffusive wave model consists of assuming that $\partial_x y \ll S$. This yields the so-called *kinematic wave equation*

$$\partial_t y + \partial_x \left(K_S |S|^{\frac{1}{2}} y^{\frac{5}{3}} \right) = w. \quad (43)$$

Equation (43) is a first-order nonlinear hyperbolic PDE. Analytical solutions can be obtained by using the method of characteristics; see, e.g., [19].

3.2 Coupling with Richards' equation

This section briefly discusses the coupling between Richards' equation (4) and the diffusive wave equation (42) in the framework of the water-table–ground interaction described in Section 2.4.

Firstly, observe that (42) is posed only on $\partial\Omega_g^+$ since $y = 0$ on $\partial\Omega_g^-$. Taking into account the mass transfer from the subsurface flow and the rainfall into the overland flow yields

$$w = u(\psi) \cdot n - v_r \cdot n, \quad (44)$$

where $u(\psi)$ is the generalized Darcy velocity in the soil and n the outward normal to Ω along $\partial\Omega_g^+$. Furthermore, assuming the vertical pressure distribution in the overland flow to be hydrostatic, the following holds:

$$\psi = y \quad \text{on } \partial\Omega_g^+, \quad (45)$$

where ψ is the matrix potential solving Richards' equation (4) and y is the overland flow height solving (42). Equation (45) replaces the boundary condition $\psi = 0$ on $\partial\Omega_g^+$ which was previously enforced for the obstacle problem.

Finally, boundary conditions must be enforced for (42). In a two-dimensional hillslope setting, $\partial\Omega_g^+$ is a segment, say $[x_{\min}, x_{\max}]$, and assume, without loss of generality, that the point with abscissa x_{\min} is located uphill and that the point with abscissa x_{\max} is located at the hillslope outlet. The following conditions can be enforced:

$$y = 0 \quad \text{at } x_{\min}, \quad (46)$$

$$\partial_x y = 0 \quad \text{at } x_{\max}. \quad (47)$$

Condition (46) is natural since it expresses the fact that the overland flow originates at x_{\min} and then flows downstream. Condition (47) is reasonable, but is harder to motivate physically; it amounts to the balance of gravitational effects and energy losses at the hillslope outlet.

Since the value of the matrix potential is now unknown over the whole ground surface, the finite element space in which the discrete matrix potential is sought is

$$P_c^1 = \{ \phi_h \in C^0(\bar{\Omega}) \cap H^1(\Omega); \forall K \in \mathcal{T}_h, \phi_h|_K \in \mathbb{P}_1 \}. \quad (48)$$

At each time step, the discrete form of Richards' equation is, for all $\phi_h \in P_c^1$,

$$\frac{1}{\delta t} \int_{\Omega} (\theta(\psi_h^n) - \theta(\psi_h^{n-1})) \phi_h + a_{(\partial\Omega_g^+)^n}(\psi_h^n, \phi_h) + \int_{(\partial\Omega_g^+)^n} \phi_h u(\psi_h^n) \cdot n = 0. \quad (49)$$

Using (44) yields

$$\begin{aligned} \frac{1}{\delta t} \int_{\Omega} (\theta(\psi_h^n) - \theta(\psi_h^{n-1})) \phi_h + a_{(\partial\Omega_g^+)^n}(\psi_h^n, \phi_h) = & - \int_{(\partial\Omega_g^+)^n} (\partial_t \psi_h + \partial_x q(\psi_h)) \phi_h \\ & - \int_{(\partial\Omega_g^+)^n} \phi_h v_r \cdot n, \end{aligned} \quad (50)$$

where the function $y \mapsto q(y)$ is defined in (41). A finite volume method can be used to discretize in time and space the right-hand side of equation (50); see [20].

4 Applications

This section presents two applications of the above finite element techniques to simulate hydrosystems, namely infiltration into a one-dimensional soil column and a two-dimensional hillslope exposed to heavy rainfall.

4.1 One-dimensional infiltration

One-dimensional stationary and unstationary infiltration problems with analytical solutions are simulated to validate the subsurface flow code.

4.1.1 Stationary test case

Consider a one-dimensional steady infiltration under a constant rainfall rate, $v_r = -ie_z$. Mass balance readily yields

$$i = k_s k_r(\psi) (\partial_z \psi + 1). \quad (51)$$

Assuming $\psi(z_L) = \psi_L$, the solution to (51) is

$$z = z_L + \int_{\psi}^{\psi_L} \frac{k_r(x)}{k_r(x) - i/k_s} dx. \quad (52)$$

The Brooks–Corey model (15) is used to express the relative hydraulic conductivity in terms of the matrix potential. Three types of soils are considered. Table 1 lists the saturation hydraulic conductivity, k_s , and the two Brooks–Corey model parameters, ψ_s and ϱ , for each soil. The left

Soil		clay	silt-loam	sand-loam
k_s	[m/h]	1.22e-3	1.22e-4	1.22e-5
$-\psi_s$	[m]	0.9	0.45	0.25
ϱ	[-]	3.3	5.64	11.88

Table 1: Saturation hydraulic conductivity and Brooks–Corey model parameters for the three soils considered in the stationary infiltration test case.

plot in Figure 3 displays the relative hydraulic conductivity as a function of matrix potential near saturation.

Using (15) in (52) yields (see, e.g., [21])

$$z = \begin{cases} z_L + g(\psi) - g(\psi_L), & \psi < \psi_s, \\ z_L + \frac{\psi_L - \psi}{1 - i/k_s}, & \psi \geq \psi_s, \end{cases} \quad (53)$$

with

$$g(x) = \psi_s G\left(\frac{i}{k_s}\right) - x G\left(\frac{i/k_s}{k_r(x)}\right) - \frac{\psi_s}{1 - i/k_s}, \quad (54)$$

where G is the hyper-geometric function $G(x) = {}_2F_1\left(\frac{1}{\varrho}, 1; 1 + \frac{1}{\varrho}; x\right)$.

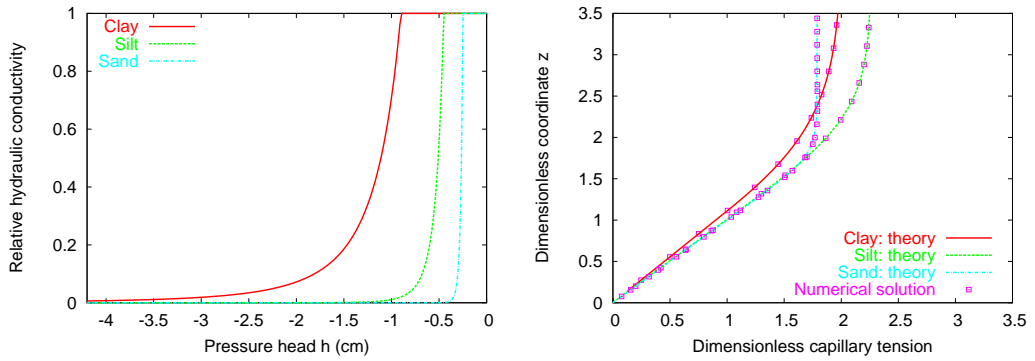


Figure 3: Stationary infiltration test case. Left: relative hydraulic conductivity k_r versus matrix potential for the three soils. Right: simulated and analytical profiles of capillary tension, $\frac{1}{\psi_s}\psi(-\frac{z}{\psi_s})$, for the three soils.

Simulations are performed with the the same infiltration rate, $i = 1.224 \times 10^{-4}$ m/h, for the three soils. The boundary condition is $\psi_L = 0$ at $z_L = 0$. The right plot in Figure 3 displays simulation results. The agreement with the analytical solution is excellent.

4.1.2 Unstationary test case

The following test case is discussed in Barry *et al.* [22]; see also [21]. Assume that the relative hydraulic conductivity is defined by the Brooks–Corey model, equation (15), with parameters ψ_s and ϱ . Let k'_r denote the derivative of the function $\psi \mapsto k_r(\psi)$. Assume that the soil water retention curve takes the following form

$$\tilde{\theta}(\psi) = \begin{cases} \gamma \int_{-\infty}^{\psi} \frac{1}{s} k'_r(s) ds, & \psi < \psi_s, \\ 1, & \psi \geq \psi_s, \end{cases} \quad (55)$$

with parameter

$$\gamma = \left(\int_{-\infty}^{\psi_s} \frac{1}{s} k'_r(s) ds \right)^{-1} = \psi_s \left(1 + \frac{1}{\varrho} \right). \quad (56)$$

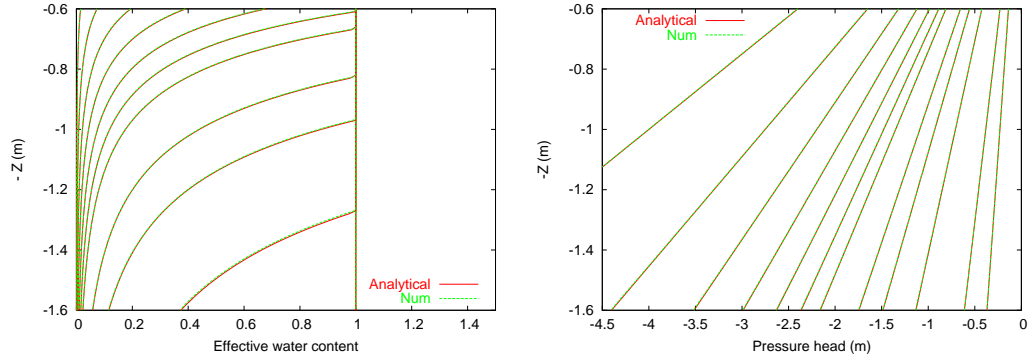


Figure 4: Unstationary infiltration test case. Simulated and analytical vertical profiles for the water content (left) and the pressure head (right) at the times $t = 10.1, 20.1, 30.1, 40.1, 50.1, 60.1, 70.1, 90.1, 100.1, 130, 170, 200, 500, 1000$ h.

Set $\mathcal{K}_s = \frac{k_s}{\theta_s - \theta_r}$ and

$$A(t) = 1 + W[-\exp(t\mathcal{K}_s/\gamma - 1)] , \quad (57)$$

where W is the lower portion of the Lambert function. Then, one can show that an analytical solution to Richards' equation, $\psi_a(t, z)$, such that $\psi_a(t, 0) = 0$ for all t , is, for $z < 0$,

$$\psi_a(t, z) = -\frac{z}{A(t)} . \quad (58)$$

Simulations are performed with the clay soil considered in the previous section ($\theta_r = 0.04$, $\theta_s = 0.432$). The simulation domain is the interval $z \in [-1.6, -0.6]$. The boundary conditions enforce the value of the analytical solution at both ends of the interval. The initial condition is the analytical solution at $t = 0.1$ h. The saturation front reaches the top boundary at about $t = 60$ h, and the domain is completely saturated at about $t = 290$ h. Results are displayed in Figure 4. The agreement with the analytical solution is very good.

4.2 Two-dimensional hillslopes

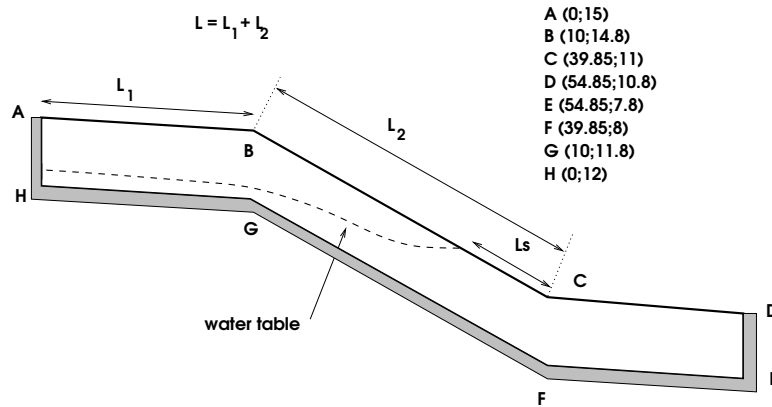


Figure 5: Hillslope geometry (length unit: meter)

Consider the two-dimensional hillslope configuration shown in Figure 5. Define $Q_{\text{rain}} = iL(e_z \cdot n)$. Let $Q_{\text{in}}(t)$ be the (time-dependent) infiltration flux and let $Q_{\text{not in}}(t)$ be the “direct

runon” flux (the water that never infiltrates); hence,

$$Q_{\text{rain}} = Q_{\text{in}}(t) + Q_{\text{not in}}(t). \quad (59)$$

Let $Q_{\text{exf}}(t)$ be the exfiltration flux and let $Q_{\text{runoff}}(t)$ consist of the exfiltration and the direct runoff fluxes

$$Q_{\text{runoff}}(t) = Q_{\text{exf}}(t) + Q_{\text{not in}}(t) = Q_{\text{exf}}(t) + Q_{\text{rain}} - Q_{\text{in}}(t). \quad (60)$$

If the rainfall intensity is kept constant in time, the time to reach equilibrium, T_e , is conventionally defined as the first time in the simulation for which

$$|Q_{\text{in}}(T_e) - Q_{\text{exf}}(T_e)| \leq 0.005Q_{\text{in}}(T_e). \quad (61)$$

At equilibrium $Q_{\text{in}}(\infty) = Q_{\text{exf}}(\infty)$ and, hence, $Q_{\text{runoff}}(\infty) = Q_{\text{rain}}$. Note that at a given time t , $Q_{\text{runoff}}(t)$ is not the instantaneous water flux at the toe of the slope but the instantaneous water flux into the overland flow.

4.2.1 Influence of the soil hydrodynamic parameters

For all the test cases presented in this section, the initial condition is the steady-state solution corresponding to a rainfall intensity of $\frac{i}{k_s} = 0.4\%$. The initial condition is presented in Figure 6. Furthermore, the obstacle model is used to simulate the water-table dynamics once it has reached the ground surface.

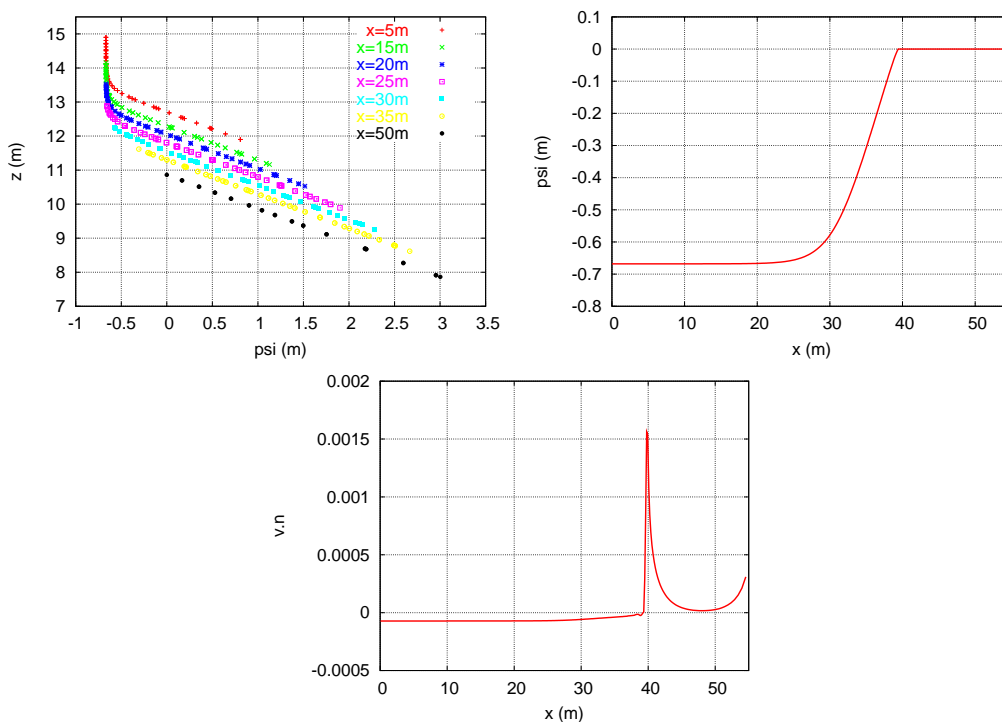


Figure 6: Initial condition for the hillslope test case. Top left: vertical profile of matrix potential at various points located by their horizontal coordinate x . Top right: matrix potential along the ground surface. Bottom: normal flow velocity along the ground surface.

We first investigate the impact of the parameters α and n in the VGM model. The soil chosen as a reference is a so-called Yolo Light Clay (YLC) soil; its VGM parameters are $\theta_r = 0.23$, $\theta_s = 0.55$, $\alpha = 3.6 \text{ m}^{-1}$, $n = 1.9$, and $k_s = 0.018 \text{ m/h}$. Then, the parameters α and n are varied,

soil	YLC	$n = 1.31$	$n = 3.9$	$\alpha = 0.3$	$\alpha = 8.0$
T_e [h]	2034	865	2925	71	3298

Table 2: Time to reach equilibrium.

and a new steady-state solution is computed. In all the simulations, the soils are subjected to a constant rainfall intensity of $\frac{i}{k_s} = 2\%$.

Times to reach equilibrium are reported in Table 2. The first line indicates the parameter that has been varied and the corresponding value. The impact of both α and n on T_e is evident. Figure 7 presents the hydrodynamic functions $\psi \mapsto \tilde{\theta}(\psi)$ and $\psi \mapsto k_r(\psi)$ for the various soils considered in the simulations. A more specific investigation of the impact of the parameter n and that of the parameter α is presented in Figure 8.

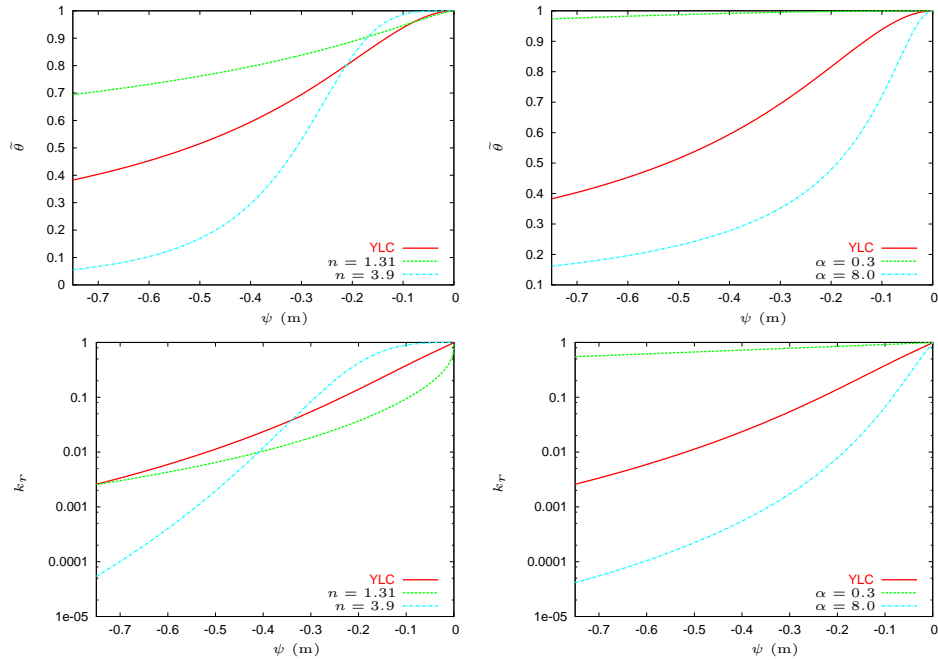


Figure 7: Hydrodynamic functions for various values of n (left) and α (right). Top: $\psi \mapsto \tilde{\theta}(\psi)$. Bottom: $\psi \mapsto k_r(\psi)$.

As a second test case, we investigate the impact of the modified VGM model on simulation results. The reference soil is again taken to be the YLC soil. Two additional simulations are performed by setting the minimum capillary height to $\psi_s = -2$ cm and to $\psi_s = -10$ cm in the modified VGM model. Figure 9 presents the corresponding hydrodynamic functions $\psi \mapsto \tilde{\theta}(\psi)$ and $\psi \mapsto k_r(\psi)$. A more specific investigation of the impact of the modified VGM model on simulation results is presented in Figure 10.

4.2.2 Influence of the overland flow

Consider the two-dimensional hillslope configuration shown in Figure 11 and investigated previously in [1]. A no-flow boundary condition is imposed at the bottom and left surfaces, simulating an impermeable layer. The right boundary corresponds to a stream in which the hydraulic head is prescribed. The initial condition is a horizontal water table located at the toe of the slope; see Figure 11. The problem geometry is characterized by the slope $S_o = 10\%$, the depth to the impermeable layer $D = 1$ m, and the length $L = 50$ m. Simulations are run with a con-

stant rainfall intensity such that $\frac{i}{k_s} = 0.6\%$. The soil hydrodynamic properties are $\theta_r = 0.069$, $\theta_s = 0.435$, $\alpha = 0.326 \text{ m}^{-1}$, $n = 3.9$, and $k_s = 5.0 \text{ m/h}$; they correspond to the sand considered in [1].

Figure 12 compares the results obtained with the obstacle model to those obtained with the model accounting for overland flow. The Strickler coefficient of roughness is set to $K_S = 10 \text{ m}^{-\frac{1}{3}}\text{s}^{-1}$. Both models yield very similar results, especially for the time evolution of the relative saturated area. Slight differences in the exfiltration flux are observed for sufficiently long times; these differences arise mainly near the toe of the slope.

References

- [1] F.L. Ogden and B.A. Watts, Saturated area formation on non convergent hillslope topography with shallow soils: a numerical investigation, *Water Resour. Res.*, **36(7)**, 1795–1804, 2000.
- [2] H.L. Cloke, J.-P. Renaud, A.J. Claxton, J.J. McDonnell, M.G. Anderson, J.R. Blake and P.D. Bates, The effect of model configuration on modelled hillslope-riparian interactions, *J. of Hydrology*, **279**, 167–181, 2003.
- [3] M. Weiler and J. McDonnell, Virtual experiments: a new approach for improving process conceptualization in hillslope hydrology, *J. of Hydrology*, **285**, 3–18, 2004.
- [4] P. Ciarlet. *The Finite Element Method for Elliptic Problems*. North-Holland, Amsterdam, 1978.
- [5] S. Brenner and L.R. Scott. *The Mathematical Theory of Finite Element Methods*. Vol. 15 of Texts in Applied Mathematics, Springer-Verlag, New York, 1994.
- [6] A. Quarteroni and A. Valli. *Numerical Approximation of Partial Differential Equations*. 2nd edition, Vol. 23 of Series in Computational Mathematics, Springer-Verlag, New York, 1997.
- [7] A. Ern and J.-L. Guermond. *Theory and Practice of Finite Elements*. Vol. 159 of Applied Mathematical Series, Springer-Verlag, New York, 2004.
- [8] J.-P. Croisille. Finite volume box schemes and mixed methods, *Math. Mod. Numer. Anal.*, **31(5)**, 1087–1106, 2000.
- [9] J. Baer and Y. Bachmat. *Introduction to Transport Phenomena in Porous Media*. Kluwer Academic Publishers, 1990.
- [10] M.Th. van Genuchten, A closed-form equation for predicting the hydraulic conductivity of unsaturated soils, *Soil Sci. Soc. Am.*, **44**, 892–898, 1980.
- [11] Y. Mualem, A new model for predicting the hydraulic conductivity of unsaturated porous media. *Water Resour. Res.*, **12**, 513–522, 1976.
- [12] T. Vogel, M. Th. van Genuchten and M. Cislerova, Effect of the shape of the soil hydraulic functions near saturation on variably-saturated flow predictions, *Advances in Water Resources*, **24(6)**, 133–144, 2001.
- [13] R.H. Brooks and A.T. Corey, Hydraulic properties of porous media, *Hydrol. Pap.*, **3**, Colorado State University, Fort Collins, p. 27, 1964.
- [14] M.A. Celia, E.T. Boulotas and R.L. Zarba, A general mass-conservative numerical solution for the unsaturated flow equation, *Water Resour. Res.*, **26(7)**, 1483–1496, 1990.
- [15] J. Lambert. *Numerical Methods for Ordinary Differential Systems*. Wiley, New York, 1991.

- [16] R. Moussa and C. Bocquillon, Criteria for the choice of flood routing methods in natural channels, *J. of Hydrology*, **186**, 1–30, 1996.
- [17] J.E. VanderKwaak and K. Loague, Hydrologic-response simulations for the R-5 catchment with comprehensive physics-based model, *Water Resour. Res.*, **37(4)**, 999–1013, 2001.
- [18] Y.B. Liu, S. Gebremeskel, F. De Smedt, L. Hoffmann and L. Pfister, A diffusive transport approach for flow routing in GIS-based flood modeling, *J. of Hydrology*, **283**, 91–106, 2003.
- [19] D.K. Borah, S.N. Prasad and C.V. Alonso, Kinematic wave routing incorporating shock fitting, *Water Resour. Res.*, **16(3)**, 529–541, 1980.
- [20] H. Beaugendre, A. Ern, T. Esclaffer, E. Gaume, I. Ginzburg and C. Kao, An obstacle-type model for the interaction of shallow water tables with ground surface, *Comput. Geosci.*, submitted, 2005.
- [21] I. Ginzburg, J.-P. Carlier and C. Kao, Lattice Boltzmann approach to Richards' equation, Proceedings of the CMWR Conference, North Carolina (2004).
- [22] D.A. Barry, J.-P. Parlange, G.C. Sander and M. Sivaplan, A class of exact solutions for Richards' equation, *J. of Hydrology*, **142**, 29–46, 1993.

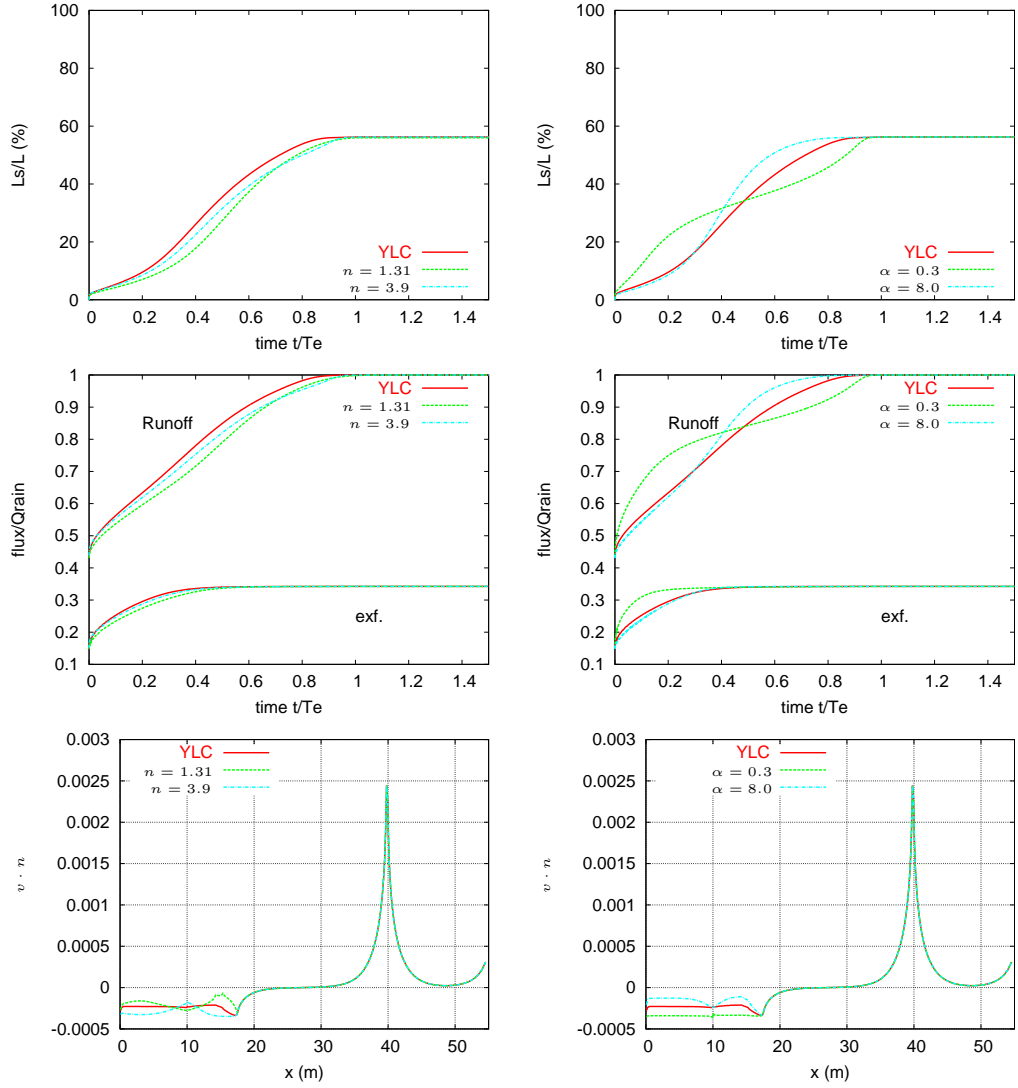


Figure 8: Left column: influence of n on simulation results; right column: influence of α on simulation results. Top: saturated length L_s normalized by length L (see Figure 5) as a function of time normalized by T_e ; middle: runoff and exfiltration fluxes normalized by Q_{rain} as a function of time normalized by T_e ; bottom: normal velocity flux $v \cdot n$ along the ground surface.

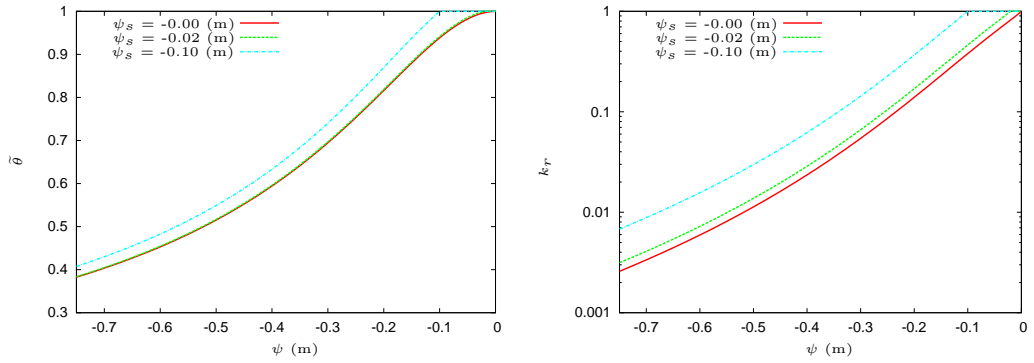


Figure 9: Modified VGM model: hydrodynamic functions for various values of ψ_s . Left: $\psi \mapsto \bar{\theta}(\psi)$. Right: $\psi \mapsto k_r(\psi)$.

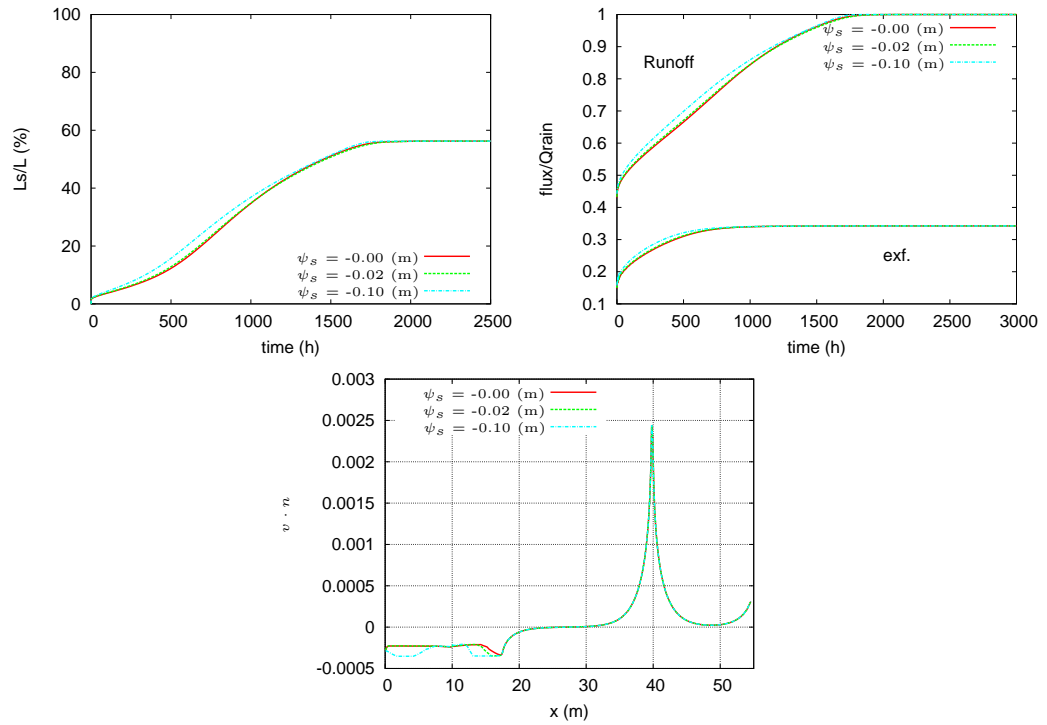


Figure 10: Impact of the modified VGM model on simulation results. Top: saturated length L_s normalized by length L (see Figure 5) as a function of time normalized by T_e ; middle: runoff and exfiltration fluxes normalized by Q_{rain} as a function of time normalized by T_e ; bottom: normal velocity flux $v \cdot n$ along the ground surface.

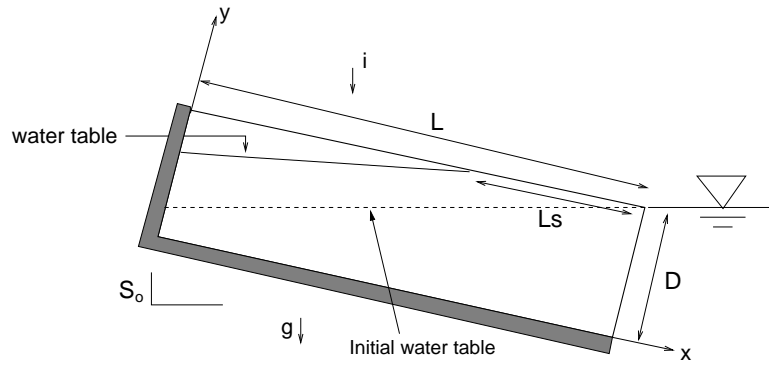


Figure 11: Hillslope geometry to compare the obstacle model with the overland flow model.

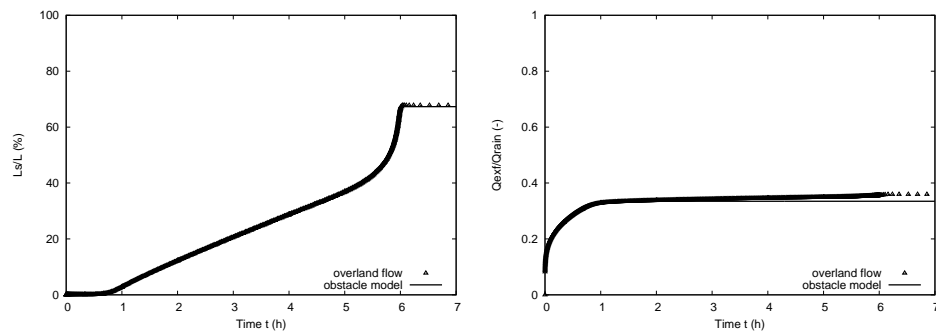


Figure 12: Comparison of the obstacle model with the model accounting for overland flow. Left: relative saturated area. Right: exfiltration flux.